New Benzimidazolyl based schiff base and its Cu(II) complexes: Crystal Structure, DFT Study, Biological Activity and Molecular Docking

Prashant Kaushik[1], Kuldeep Mahiya[2], Mandeep[3], Presenjit[4], Ritika[5], Vinod Kumar[6], Ajay Kumar Mishra[7], Swaraj kumar babu[8], Pradeep Kumar Naik[8], Ravinder Kumar[1]*

[1]Deaprtment of Chemistry, Gurukula kangri (Deemed to be University), Haridwar-249404, India; [2]Department of Chemistry, FGM Government College, Adampur, Mandi Adampur, Hisar-125052 Haryana, India, [3]Department of Chemistry, Dyal Singh College, Karnal-132001, Kurukshetra University, India, [4]Department of Chemistry, Babasaheb Bhimrao Ambedkar University (A Central University), Lucknow–226025, India, [5]Dr. B.R Ambedkar Center for Biomedical Research, University of Delhi, Delhi–110007, India; [6]Department of Chemistry, University of Delhi, Delhi-11007, India, [7]Department of Chemistry, University of the Western Cape, South Africa, [8]Department of Biotechnology and Bioinformatics, Sambalpur University, Jyoti Vihar , Burla, Sambalpur-768019, Odisha, India.

***Corresponding authors**: ravinder.kumar@gkv.ac.in

Abstract

Two novel copper complexes with the novel benzimidazole based ligand (4-((2-(1H-benzo[d]imidazol-2-yl)ethylimino)methyl)benzene-1,3-diol) (AB-DHB) have been synthesized and characterized by UV-visible spectroscopy, FT-IR, ^{13}C NMR, ^{1}H NMR, SEM with EDX measurement, PXRD technique and SCXRD. SCXRD analysis of ligand shows the intra and intermolecular hydrogen bonding present in the molecule. The ligand behaves as a tridentate. Both complexes have distorted square planar geometry for the Cu(II) ion with Cl- and Br-. Cytotoxicity assays against MCF-7 breast cancer cells revealed potent anticancer effects, with the Cu(L)Cl complex exhibiting the most significant activity, outperforming both the free ligand and Cu(L)Br. Anti-inflammatory studies using TNF-α and IL-6 cytokine assays showed dose-dependent inhibition, where Cu(L)Cl shows the highest inhibition (56.52%) at lower concentration (50 µg/mL). The antifungal activity against *Fusarium oxysporum* indicated a consistent increase with concentration; Cu(L)Br displayed slightly better inhibition (52.65 ± 3.37%) than Cu(L)Cl (50.97 ± 3.19%) at 1.5 mg/mL, suggesting a role of halide lipophilicity in fungal membrane

disruption. Antioxidant activity, assessed via the DPPH assay, showed that the ligand had the highest scavenging ability ($IC_{50} = 1.12 \times 10^{-4}$ g/mL), followed by Cu(L)Cl and Cu(L)Br, indicating efficient radical quenching facilitated by hydroxyl groups. Molecular docking studies supported the experimental data, where Cu(L)Cl showed strong binding to the anti-apoptotic Bcl-2 protein (2W3L) with a docking score of –6.06 kcal/mol, and the ligand exhibited high affinity toward HO-1 (1N3U) with a score of –7.89 kcal/mol. These findings underscore the therapeutic promise of ligand and copper(II) complexes as potent, multi-target agents with anticancer, anti-inflammatory, antifungal and antioxidant properties.

Keywords: Benzimidazole ligand, Single Crystal, Complexes, DFT and Biological activity

1. Introduction

Cancer is the most deadly diseases for humans, and there is presently no effective treatment available. Cancer is a disease that causes a person's cells to spread out of control and propagate to other body parts. Cancer can spread throughtout the body's billions of cells [1]. Among the most prevalent cancers is breast cancer. The second leading cause of death for women is breast cancer, which is also the most prevalent type of cancer [2]. In most nations, the leading cause of death is cancer [3]. In the past several years, about 500 men and 41,760 women have lost their lives caused by breast cancer, as per the American Cancer Society (ACS)[4]. Ductal carcinoma and lobular carcinoma are the two subtypes of breast cancer. It is defined as an aberrant proliferation or division of epithelial cells within a lobe or lactiferous duct[5].

Benzimidazole is a bicyclic molecule that is created when imidazole and benzene are combined. It is a significant pharmacophore and a desired structure in pharmaceutical chemistry[6,7]. The benzimidazole moiety is essential in the pharmaceutical industry for the creation of novel medications[8,9]. Metal complexes of benzimidazole derivatives play a significant role in organic transformations as well[10–18]. Benzimidazole derivatives exhibit significant pharmaceutical properties such as anti-fungal[19], anti-bacterial[20], anti-proliferative[21], anti-viral[22,23], anti-ulcer[24], anti-HIV[25], anti-oxidant[26,27], anti-cancer[28], anti-diabetic[29], and anti-tumor[30–32] (Fig. 1.).

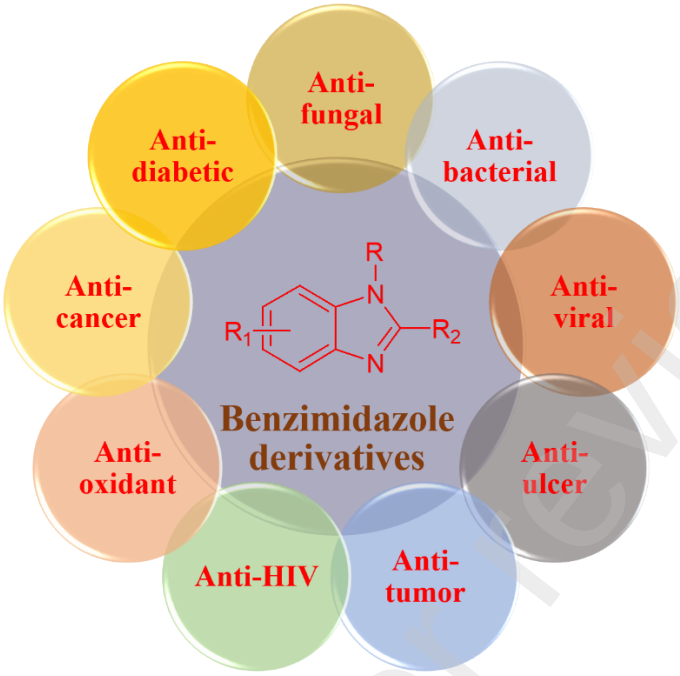

Fig. 1. Pharmaceutical properties of benzimidazole derivatives.

In the human body, copper is a necessary metal that is engaged in numerous vital biological processes. It displays a variety of coordination numbers and shapes, along with redox features that are individually intriguing. Because of these characteristics, copper complexes are particularly appealing for the search for pharmacologically active molecules, particularly in the area of cancer research[33]. Metal compounds have been used in medicine since the 16th century when studies on the medicinal use of metal-containing compounds or metals in the treatment of cancer were published. These days, antimony (anti-protozoal)[34], bismuth (anti-ulcer)[35,36], iron (anti-malarial)[37], platinum (anti-cancer)[38], silver (anti-microbial)[39], gold (anti-arthritic)[40], and vanadium (anti-diabetic)[41] are among the medicinally recommended metal-containing compounds. A common tendency of metal ions is to interact and bind to a variety of vital biological components because they lack electrons, whereas the majority of biological compounds (such as proteins and DNA) include electrons.

Additionally, metal ions have a strong attraction for a variety of tiny molecules that are essential to life, such as O_2. Much of the previous and present interest in creating novel ways to use metal-containing compounds or metals to modify biological systems has been driven mainly by these reasons. A set of complex substances, including 2-aminobenzimidazole derivatives and metals including cobalt, nickel, and copper revealed antibacterial and antifungal activities[42,43].

This work's main objective is to examine the benzimidazole ligand's (AB-DHB) coordination behavior which includes several Cu(II) binding sites. At room temperature, UV-vis, IR, ^{1}H NMR, ^{13}C NMR, SEM with EDX measurement, PXRD and single crystal XRD technique were used to determine the structures of benzimidazole-based ligand (AB-DHB) and both copper (II) complexes. The biological activity of the ligand and copper(II) complexes persented here is also reported.

2. Experimental

2.1. Materials and methods

O-phenylenediamine (AVRA Mumbai), β-alanine (thermo fisher), K_2CO_3 (thermo fisher), 2,4-dihydroxy benzaldehyde (Induschembio), $CuCl_2.2H_2O$ (labachemie), $CuBr_2$ (Induschembio), were used as obtained. FBS (Fetal Bovine Serum), DMEM (Dulbecco's Modified Eagle Medium), streptomycin, penicillin, and trypsin solution were purchased from GIBCO, DMSO, and MTT dye. The process described by Cescon and Day was followed in the synthesis of 2-aminoethylbenzimidazole dihydrochloride[44].

A Shimadzu UV-Vis-2550 spectrometer was used to record the UV-visible spectra in MeOH at Gurukula Kangri (Deemed to be University), Haridwar. A Perkin-Elmer FT-IR-2000 spectrometer was used to record IR spectra using KBr discs within the 400–4000 cm^{-1} range. ^{1}H and ^{13}C NMR were done on Bruker 600 MHz system at Institute Of Nuclear Medicine & Allied Sciences (INMAS) nmr facility New Delhi. The morphology of the ligand (AB-DHB) and complexes were investigated using SEM with the gold coating (Zeiss, Model EVO 18 Special Edition, Germany) in the IIT Roorkee research lab in India. A multimode microplate reader (VICTOR Nivo, Perkin Elmer) was used to get UV absorbance values.

2.2. Synthesis of Ligand

2-aminoethyl-benzimidazole dihydrochloride synthesized by the following procedure reported by Cescon *et. Al.* The aqueous solution (15 mL) of 2-aminoethyl-benzimidazole dihydrochloride (AB.2HCl, 1.5g, 6.4 mmol) was neutralized by adding the appropriate amount of aqua. K_2CO_3 and filter it. A 10 ml MeOH solution of 2,4-Dihydroxybenzaldehyde (0.88 g, 6.4 mmol) was then added dropwise to the filtrate while being continuously stirred at room temprature.

After 5 min of stirring the precipitate was formed. The resulting precipitate was vacuum-dried on anhydrous $CaCl_2$ after being repeatedly cleaned with cold water (Scheme 1).

M.W. 281, Yield: 60% Selected IR(KBr, cm^{-1}): $\upsilon_{(NH)}$ 3444, $\upsilon_{(-C=N-C=C-C-)}$ 1449, $\upsilon_{(C-O)}$ 1254, $\upsilon_{(-HC=N-)}$ 1646, $\upsilon_{(-OH)}$ 2853, $\upsilon_{ring\ pulsation}$ 748. . ^1H NMR (400 MHz, DMSO-d_6, δ ppm): 13.60(s, 1H, OH), 12.30(s, 1H, OH), 10.02(s, 1H, NH), 8.38(s, 1H -CH=N-), 7.47–6.12(s, 7H, aromatic), 3.99(s, $-CH_2-$), 3.15(s, $-CH_2-$).^{13}C NMR (100 MHz) (ppm) (DMSO-d_6): 165.8, 165.02, 162.22, 153.31, 133.8-103, 55.59, 30.80. UV–Vis λ_{MAX} in MeOH: 274, 280, 303, 363.

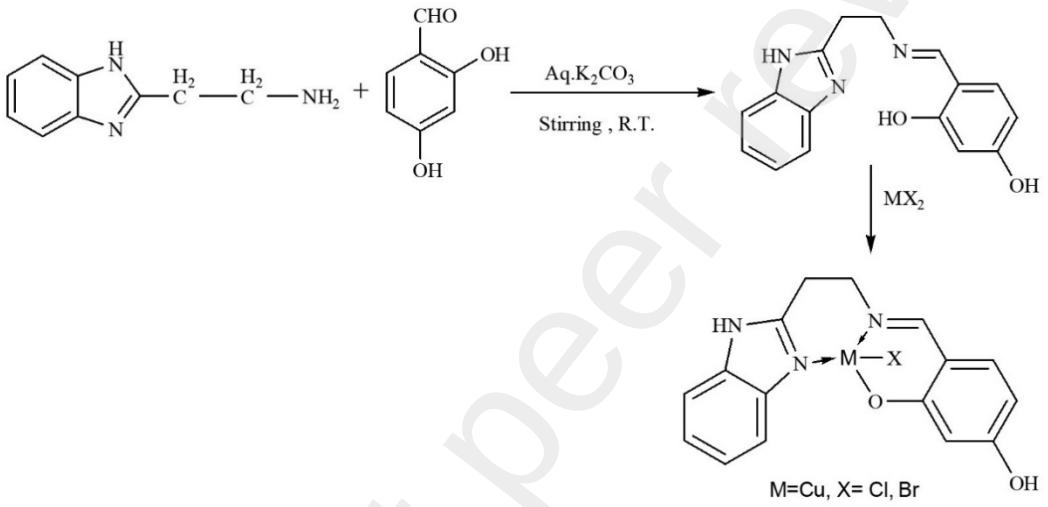

Scheme 1. Synthesis of ligand AB-DHB and copper(II) complexes

2.3. Synthesis of [Cu(L)Cl] and [Cu(L)Br]

Ligand (AB-DHB) (100mg, 0.354 mmol) dissolved into 20 ml methanol. 10 ml MeOH solution of $CuCl_2.2H_2O$ (60.28 mg, 0.354 mmol) was added dropwise into the pre-dissolved hot MeOH solution of the ligand with constant stirring at 25°C. A green-colored solution generated instantly during addition. After 2 hours of stirring, the green color solution was put into the air for slow evaporation of methanol. After 3/4 days green colored precipitate formed and filtered. The precipitate was air-dried in a vacuum over CaCl2 after being cleaned with cold MeOH Scheme 1. Cu(L)Br was synthesized by following the same technique as Cu(L)Cl except that copper (II) bromide (79.2 mg, 0.354 mmol) was used for complexation. The green precipitate was collected and filtered. The precipitate was air dried in a vacuum over CaCl2 after being cleaned with cold MeOH.

[Cu(L)Cl] Selected IR(KBr, cm^{-1}): $\upsilon_{(NH)}$ 3337, $\upsilon_{(-C=N-C=C-C-)}$ 1454, $\upsilon_{(C-O)}$ 1230, $\upsilon_{(-HC=N-)}$ 1618, $\upsilon_{(-OH)}$ 3191, $\upsilon_{ring\ pulsation}$ 746. UV–Vis λ_{MAX} in MeOH: 278, 283, 353, 449, 650 nm.
[Cu(L)Br] Selected IR(KBr, cm^{-1}): $\upsilon_{(NH)}$ 3337, $\upsilon_{(-C=N-C=C-C-)}$ 1454, $\upsilon_{(C-O)}$ 1227, $\upsilon_{(-HC=N-)}$ 1619, $\upsilon_{(-OH)}$ 3122, $\upsilon_{ring\ pulsation}$ 748. UV–Vis λ_{max} in MeOH: 272, 278, 355, 449, 660 nm.

3. Results and discussion

3.1. Spectroscopic Studies

The UV-visible spectrum of the ligand (AB-DHB) and the Cu(II) complexes in HPLC gradient MeOH are given in (Fig. S1.). The ligand HL has four separate absorption peaks at 274, 280, 303, and 363nm which were shifted to between 278 nm, 353-355nm, and 448-453 nm, respectively, in the Cu(II) complexes. Because of the d^9 configuration of copper(II), a wide but significantly lesser intensity d-d band is detected in complex 1, and 2 at 650, and 661 nm respectively (Fig. S2.). The Cu(II) ion in both the complexes are distorted square planar in geometry[8].

The ligand infrared spectra revealed a strong band in the 3337-3444 cm^{-1} range caused by $NH_{benzimidazole}$ that remained constant after complexation, which indicates that it did not participate in complex formation[45]. A sharp band of about 1646 cm^{-1} was ascribed to the υ(C=N) stretch[10,16,17], while the band resulting from the ligand υ(OH) stretching vibration was determined to be a strong band of nearly 2853 cm^{-1}. The formation of multiple medium-intensity bands in the 2500-2700 cm^{-1} range indicates the presence of hydrogen bonds between the benzimidazole's NH and other ligand's electronegative atoms[45] (Fig. S3.). These bands are also seen in complexes, which suggests that hydrogen bonds exist there as well. (Table S1) contains the benzimidazole-based ligand (AB-DHB) and their copper complexes' infrared data. The coordination sites that might be involved in chelation are identified by comparing the infrared spectra of the complexes and the ligand (AB-DHB). The ligand exhibited neutral tridentate ligand behavior in both complexes, coordinating through one hydroxyl group (NNO) and two imine groups. Both complexes' infrared (IR) measurements showed that the band corresponding to the imine group had changed to a lower wave number. And υ(C-O), as well as a reduction in intensity, indicating that it assists in coordination. The new bands in the 468-483 and 600-598 cm^{-1} ranges of both complexes spectra were indicated to (M-N) and (M-O) vibrations, respectively[46,47].

3.2. NMR Studies of the Ligand

^{1}H NMR Spectra of ligand (AB-DHB) was taken in dimethylsulfoxide-d6 (DMSO-d6) (Fig. S4.). The ligand's ^{1}HNMR spectra revealed three signals at 13.60, 12.30, and 10.02 ppm. The signal at 13.60 and 12.30 ppm is assigned to the phenolic OH while the signal at 10.02 ppm was associated with $NH_{imidazole}$. The singlet at 8.38 ppm was ascribed to the -CH=N- proton[45]. The findings in the 7.47-6.12 ppm range could be attributed to aromatic ring protons. The signal from two $-CH_2-$ molecules showed as a singlet at 3.99 and 3.15 ppm.

In ^{13}C NMR peaks at 165.8 ppm and 165.02 ppm were ascribed to the -OH group whereas the peak at 162.22 ppm assigned azomethine (-CH=N-) group[48]. A peak between 133.8-103 ppm showed aromatic carbon[49]. Peak at 55.59 ppm and 30.80 represented the aliphatic carbon (Fig. S5.).

3.3. Morphological Analysis

The morphology of the synthesized ligand (AB-DHB) and Copper (II) complexes was examined with the SEM in Fig. 2. Gold-coated samples of the AB-DHB and Copper(II) complexes were used in SEM measurements. Fig. 2A. shows the SEM image of the ligand AB-DHB. AB-DHB shows needle-like morphology. The surface morphology variation for metal complexation of ligands with metal ions is depicted in the micrographs. After the complexation of ligand (AB-DHB) needle-like morphology is converted into cubes and rods. Cu(L)Cl (Fig. 2B.) shows cube-like morphology while Cu(L)Br (Fig. 2C.) shows rectangular plate-like morphology.

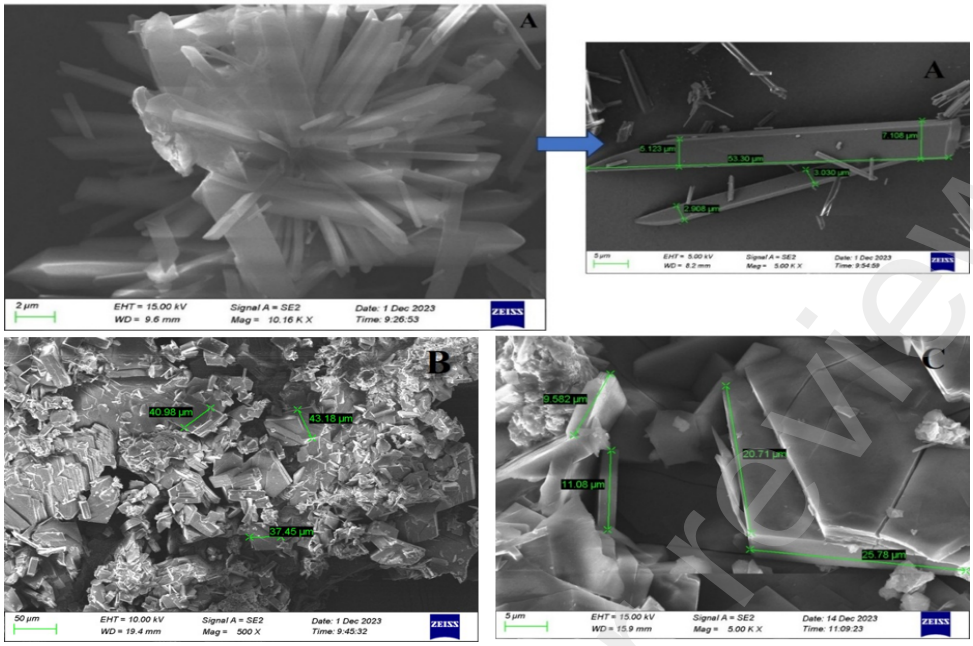

Fig. 2. SEM Image of ; (A) Ligand (AB-DHB), (B) Cu(L)Cl complex, (C) Cu(L)Br complex

EDX analysis confirms the purity of the ligand (AB-DHB) and copper complexes. (Fig. S6A.) shows a consistent arrangement of C, N, and O components in the ligand (AB-DHB). (Fig. S6B., S6C.) shows an equitable arrangement of C, N, O, Cl, and Cu elements in the copper complexes. As a result, the prepared samples have a pure elemental composition.

3.4. Single crystal analysis

The orange needlelike single crystals were obtained from methanol and water solution (1:1) of ligand after slow evaporation. Fig. S7. shows a digital image of ligand crystal that has been mounted for single crystal XRD investigation. The ligand single crystal structure demonstrates that one hydrogen atom attaches itself to the imine's N atom after being deprotonated from the hydroxyl group.The benzyl ring partial double bond nature, which correlates to the keto–enol tautomeric bond between the azomethine group's nitrogen and the benzyl's oxygen, is suggested by the bond length of the C–O group, which is 1.2957(15) in Fig. 3. The hydrogen on azomethine nitrogen forms intramolecular H-bonds with benzaldehyde oxygen, N1-H....O1 (1.939Å) in Fig. 4. Which suggest that, the oxygen at ortho position is availble to bound metal atom in metal complaxation. Table S2 provides ligand crystal data and structural refinement. Tables S3 and Table S4 indicate the bond distances and angles between the atoms. The molecule forms a symmetrical

hydrogen bonded dimer via intra and intermolecular N-H…O hydrogen bonding. ORTEP diagram in Fig. 4. showing the intra and intermolecular hydrogen bonding present in the molecule. Diagram Fig. 5. showing the intermolecular hydrogen bonding of central hydrogen bonded dimer with four neighboring hydrogen bonded dimers (*left*) and formation of a 2-D sheet viewed along crystallographic *a*-axis (*right*). Fractional atomic coordinates and anisotropic displacement parameters for ligand are mentioned in Table S5 and Table S6. The hydrogen bonds (Table S7), torsion angles (Table S8), hydrogen atom coordinates and isotropic displacement parameters (Table S9) of ligand also mentioned in supplementrory file.

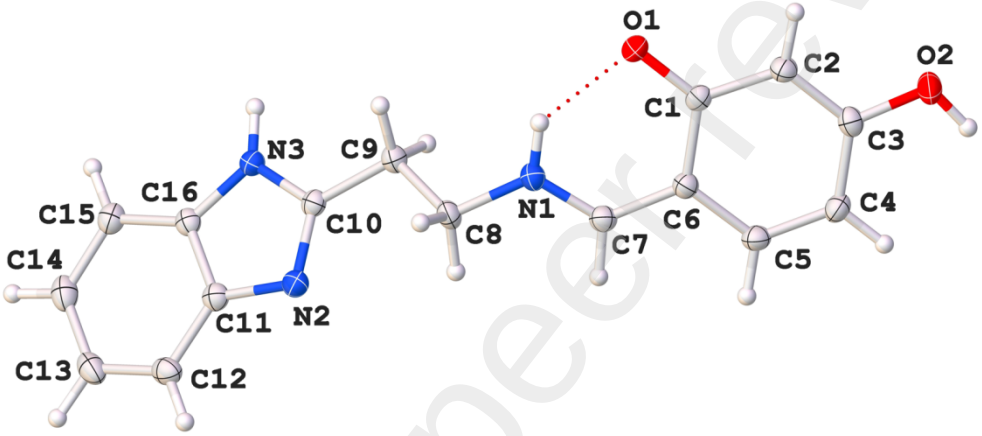

Fig. 3. An ORTEP diagram of the ligand that displays the atomic numbering scheme is depicted in 505 thermal probability ellipsoids.

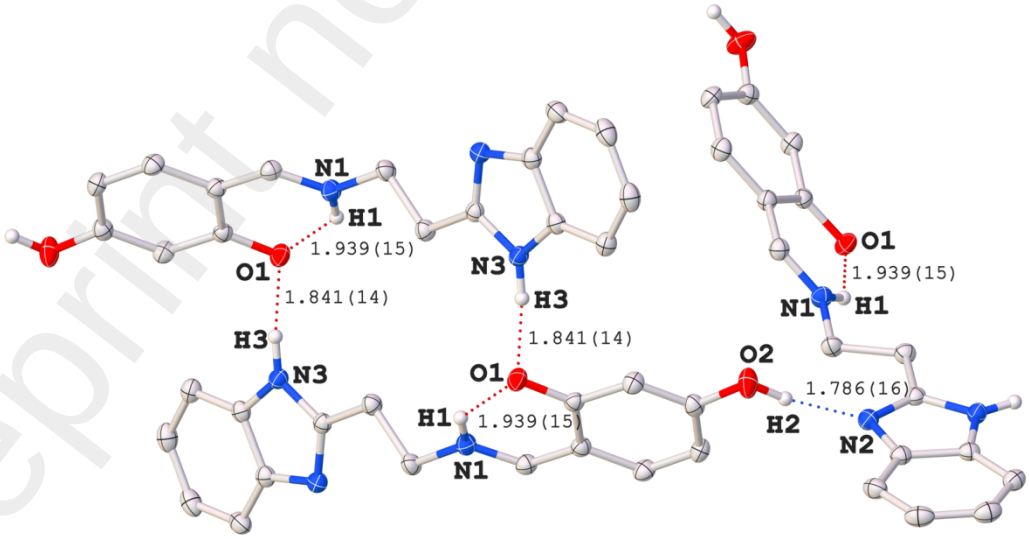

Fig. 4. The ORTEP diagram illustrates the molecule's intramolecular and intermolecular hydrogen bonds.

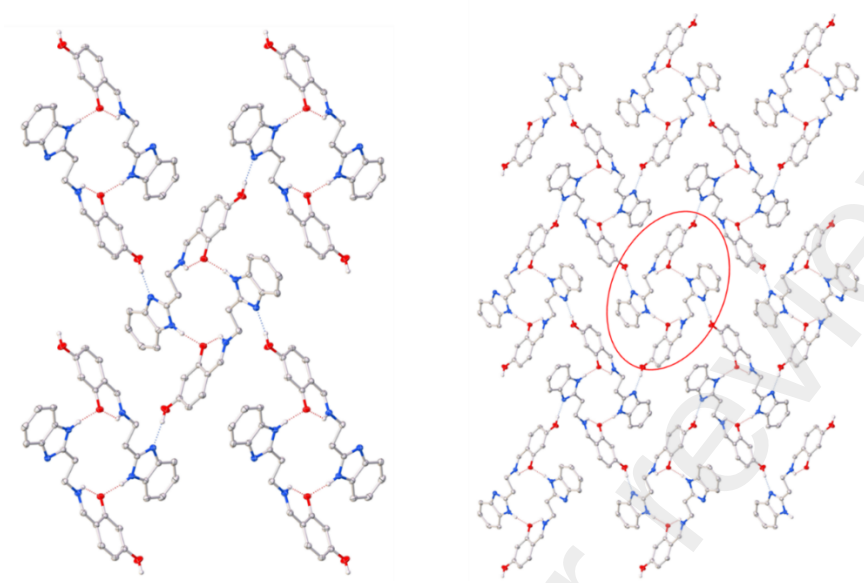

Fig. 5. The intermolecular hydrogen bonding diagram of central hydrogen bonded dimer with four neighboring hydrogen bonded dimers (*left*) and formation of a 2-D sheet viewed along crystallographic *a*-axis (*right*).

3.5. DFT Computational Study

In this work, The Materials Studio 5.5 software package from Accelrys Inc. contained the DMol3 code, which was used for all first-principles density functional calculations[50]. For better accuracy, the numerical basis set of DNP (double zeta quality plus polarization) functions was employed. To study the weak interactions, Grimme's method for DFT-D2 correction [51] was used with GGA-PBE [52] functional in all DFT calculations.

In DFT studies, first of all, we optimize the structure of ligand and complexes with local minima as shown in Fig. 6. Before studying the binding energy between ligand and copper metal atom in different complexes, we observed the HOMO and LUMO plots of all the substrates and their energy gap. An essential component of a substrate's chemical reactivity is the HOMO-LUMO [53].

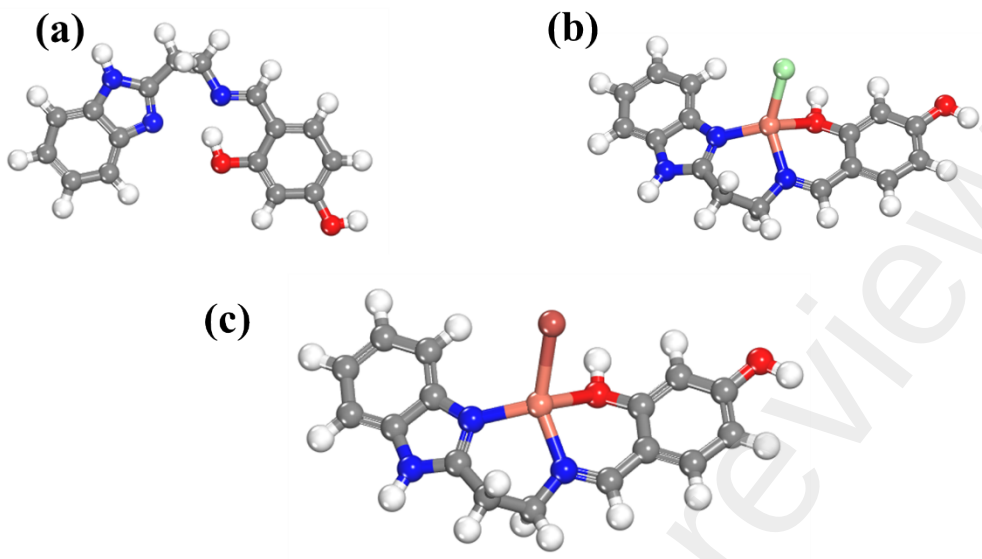

Fig. 6. Optimized structure of (a) ligand AB-DHB (b) Cu(L)Cl (c) Cu(L)Br; (Colour Code: Gray: Carbon; Red: Oxygen; Green: Chlorine; White: Hydrogen; Blue: Nitrogen; Brown: Bromine; Rust: Copper)

The HOMO-LUMO plots are given in Fig. 7. and Table 2 shows their respective energies. In the HOMO-LUMO plot of ligand AB-DHB, it is found that the HOMO plot mainly lies over the electron-rich carbon atom with the electronegative oxygen and nitrogen atoms. The LUMO plot lies on the electron-deficient carbon atoms and anti-bonding orbitals of oxygen and nitrogen atoms (Fig. 7a.). In Cu(L)Cl, it is observed that a HOMO plot exists over copper, chlorine, oxygen, and nitrogen atoms and LUMO lies on electron-deficient carbon atoms and anti-bonding orbitals of oxygen and nitrogen as shown in Fig. 7b. In Cu(L)Br, the HOMO plot is observed on bromine, oxygen, and nitrogen atoms with copper metal atoms, as shown in Fig. 7c. The LUMO plot of complex 2, lies mainly on the electron-deficient carbon atoms with anti-bonding orbitals of oxygen and nitrogen. Table 2 shows the HOMO-LUMO energy gap.

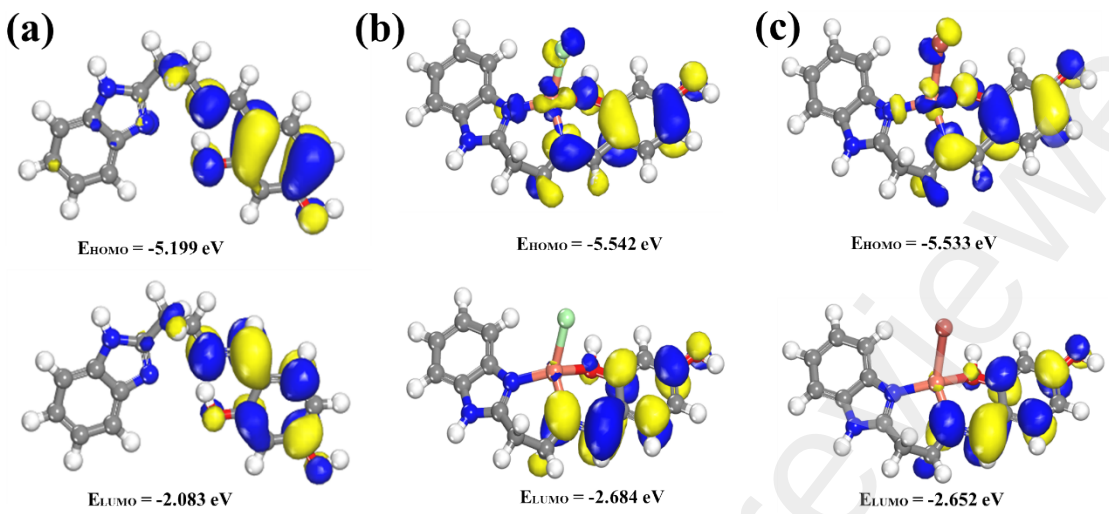

Fig. 7. HOMO and LUMO plots of the (a) ligand, (b) Cu(L)Cl, (c) Cu(L)Br

Table 2. HOMO-LUMO energy of ligand and copper(II) complexes.

S.N.	Substrates	HOMO (eV)	LUMO (eV)	HOMO-LUMO Energy Gap (eV)
1.	Ligand (AB-DHB)	-5.199	-2.083	3.116
2.	Cu(L)Cl	-5.542	-2.684	2.858
3.	Cu(L)Br	-5.533	-2.652	2.881

Further, we studied the binding energy between copper metal atom and the ligand in different complexes. The binding energy of substrates is calculated by the following equation.

$E_{BE} = E_{Complex} - E_{Ligand} - E_{Cu/Cl/Br}$

Where E_{BE} is the binding energy.

$E_{Complex}$ is the overall energy of the complex.

E_{Ligand} is the total energy of the ligand (AB-DHB).

$E_{Cu/Cl/Br}$ is the total energy of the Copper, Chlorine, and Bromine.

After calculating the binding energy, we found that the binding energy is higher for Cu(L)Cl as compared to the binding energy of Cu(L)Br. The negative value of binding energy is a justification for the stability of both the complexes as shown in Table 3.

Table 3. The binding energy of ligand with different substrates.

Sr. No.	Substrate	Binding Energy (eV)
1.	AB-DHB/CuCl (Complex 1)	-2.853
2.	AB-DHB/CuBr (Complex 2)	-2.603

3.6. Stability of the complexes in MeOH solution

The stability of complexes is a crucial measure of their validity. The stability of the compounds in solution was tracked using electronic absorption spectroscopy for either 6 or 90 hours. In MeOH, Cu(L)Cl and Cu(L)Br UV-Vis spectra were captured. Both complexes were stable in the MeOH solution for 6 and 90 hours under the specified conditions, according to the results. The scanning kinetics that were achieved are shown in Fig. S8. Both compounds showed evidence of the d-d transitions band. The UV-Visible absorption spectra of copper(II) complexes in MeOH solutions were monitored and recorded for 90 hours. The shape of the spectra did not vary much over time, as seen in Fig. S7. The d-d band was likewise visible in both complexes for 90 hours (Fig. S9). Under ideal conditions, the decrease in absorbance is most likely caused by precipitation (which is invisible to the naked eye).

4. Biological Applications

4.1. MTT assay

The MTT assay was implemented to thoroughly evaluate the cytotoxicity of the synthesized compounds on human embryonic kidney (HEK 293) and human breast cancer (MCF-7) cell lines. Four thousand cells per well were seeded into a 96-well plate, and the plate was incubated at 37ºC according to a previously published protocol[54]. Subsequently, the cells were exposed to varying concentrations (ranging from 1mM to 100µM) of the ligand (AB-DHB) and both complexes at 37ºC and 5% CO_2 for 24, 48, and 72 hours. After adding the 3-(4, 5-dimethyl-2-thiazolyl)-2, 5-diphenyl-2H-tetrazolium bromide (MTT) reagent (0.05 mg/ml) to each well (treated and control) at varying intervals, the wells were incubated for three hours at 37ºC. After cell lysis, the media from each well were decanted, and 150 µL DMSO was added to solubilize the formazan crystals. At 570 nm, the optical density was measured. This experiment was performed in triplicate to ensure the results were reliable and reproducible.

4.2. Cytotoxicity Analysis

The MTT assay, which was employed to calculate the cytotoxicity of the synthesized compounds on the HEK-293 and MCF-7 cell lines, produced positive findings. After treatment with HEK cells for 24 hours, the ligand (AB-DHB) and complex 1, 2 at a concentration of 1nM caused very little cell lysis, just 0.82 0.65, and 0.86 respectively. Likewise, 7.35, 7.37, and 10.32 of HEK and cells died after a 24-hour treatment with 100µM compounds, and even after 72 hours, the observed cell death rose to just 10.11, 9.24, and 11.06 respectively. These findings showed that all the compounds are non-toxic to HEK cell lines. Importantly, a concentration-dependent cytotoxicity trend was observed, although the levels were not excessively high, even after an extended incubation period of 48 and 72 hours. However, when the treatment of all the compounds was done with the MCF-7 cell line, great toxicity was observed. After treatment with MCF-7 cell lines for 24h, the ligand (AB-DHB) and complex 1, 2, at a concentration of 1nm showed very good cell death, 39.83 49.3, and 40.79, respectively. Similarly at 100µM compounds showed 50, 58.63, and 48.24 cell death. After 72h incubation, the cell death rose to 55.91 54.46, and 59.44 respectively at 100µM concentration. The data confirm the compound's biocompatibility by showing no appreciable cytotoxicity on the HEK cell line for up to 72 hours and showed great toxicity to the MCF-7 cell line. The study was repeated out three times in triplicate, and the results, which are shown in Fig. 8. and Fig. 9., were effectively reproducible.

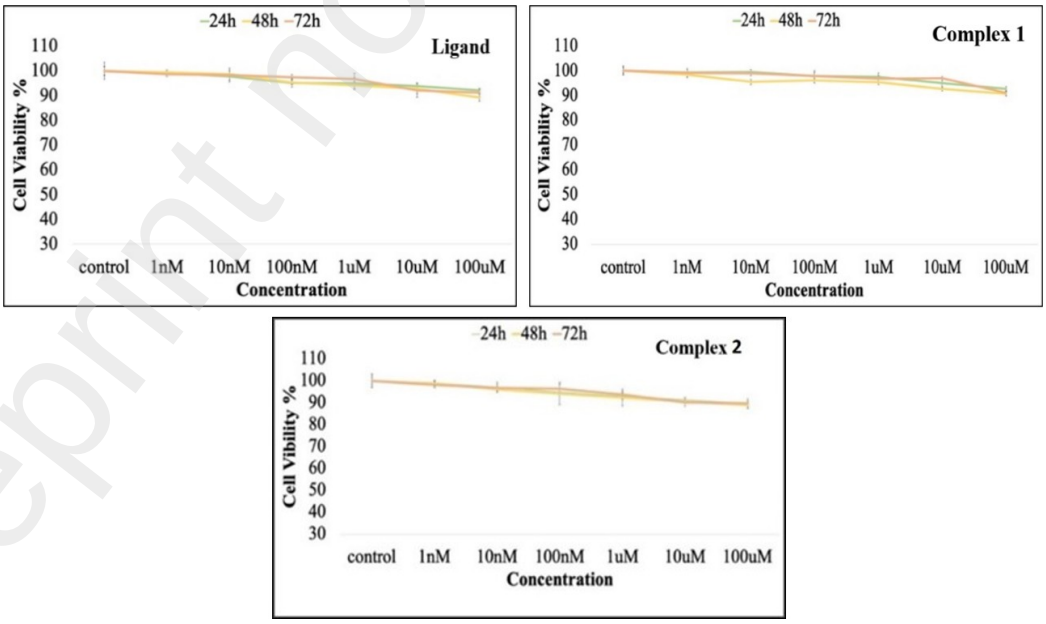

Fig. 8. Cytotoxicity of the ligand (AB-DHB) and its copper(II) complexes on HeK cells.

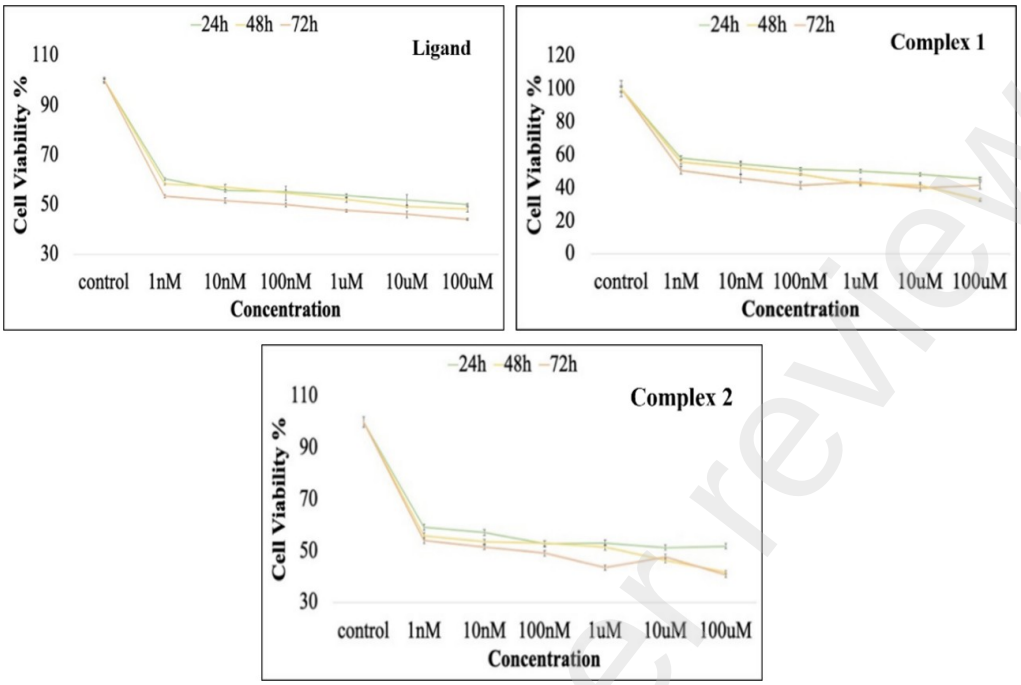

Fig. 9. Cytotoxicity of the Ligand (AB-DHB) and their copper(II) complexes on MCF-7 cells

The IC_{50} values calculated for the samples revealed that all compounds can inhibit the proliferation of breast cancer cells (MCF-7). The free ligand exhibited moderate cytotoxicity**,** with an IC_{50} value of 6.30×10^{-8} g/mL, whereas both copper complexes showed significantly enhanced activity. The Cu(L)Cl complex emerged as the most active, with an IC_{50} of 1.58×10^{-8} g/mL, followed by Cu(L)Br at 3.16×10^{-8} g/mL. This notable enhancement is likely due to increased lipophilicity and membrane permeability, along with the ability of copper to undergo redox cycling**,** producing intracellular reactive oxygen species (ROS) that trigger apoptosis via oxidative stress pathways[45].

4.3. Anti-inflammatory Antifungal, and antioxidant activity

The ligand and copper(II) complexes showed storng anti-inflammatory activity by the inhibiting formation of tumor necrosis factor-alpha (TNF-α) in J774. A.1 cells. The treatment of cells with lipopolysaccharide (LPS) considerably raised the levels of tumor necrosis factor-alpha (TNF-α), making it a positive control group (cells with LPS induction) compared to control untreated cells (cells without LPS induction). The ligand and copper(II) complexes showed significant inhibitory effects on the production of TNF-α (Table S10). It is further evidence that the administration of test compounds, at different dose of 12.5-200 µg/ml, successfully inhibited the production of

interleukin-6 (IL-6) in J774.A1 cells, a marker for anti-inflammatory activity at a dose dependent manner (Table S11). Lipopolysaccharide (LPS) injection to J774.A1 cells significantly raised IL-6 concentrations compared to the control group (J774.A1 cells not treated with LPS). The anti-inflammatory activity of the ligand and its Cu(II) complexes on TNF-α and IL-6 show concentration-dependent patterns. At lower doses (12.5-50 µg/mL), Cu(L)Cl inhibits TNF-α more effectively (13.08-53.94%) than the ligand (6.44-42.28%) and Cu(L)Br (5.75-39.28%), indicating that the Cu-Cl bond increases electronic interactions and promotes better binding with TNF-α targets. But as the concentration rises, both the ligand and Cu(L)Br exhibit similar and noticeably greater activity (TNF-α: 97.59% and 97.92% at 200 µg/mL, respectively) than Cu(L)Cl (85.68%). This suggests that the ligand's free –OH groups and the advantageous helogen binding effects, polarizability of the Cu–Br bond sustain high cytokine inhibition efficiency at higher doses[55,56].

At low concentrations (2.55–5.63% at 12.5–25 µg/mL), all drugs exhibit modest suppression of IL-6, with little variation between them. The ligand gives the maximum inhibition (75.16%) at 200 µg/mL, followed by Cu(L)Br (72.22%) and Cu(L)Cl (48.02%). Activity increases gradually with increasing concentration. This emphasizes the importance of the free hydroxyl group in the ligand, which is still available for hydrogen bonding and radical quenching, resulting in higher IL-6 suppression than its complexes. Cu(L)Cl inhibits TNF-α more effectively at lower concentrations, but the ligand and Cu(L)Br outperform at higher concentrations, especially against IL-6, where the ligand has the largest inhibitory impact. Table 4 shows the %inhibition of ligand and complexes for TNF-α assay and IL-6 assay.

Table 4 shows the %inhibition of ligand and complexes for TNF-α assay and IL-6 assay.

Conc. (µg/mL)	Ligand (TNF-α)	Cu(L)Cl (TNF-α)	Cu(L)Br (TNF-α)	Ligand (IL-6)	Cu(L)Cl (IL-6)	Cu(L)Br (IL-6)
12.5	6.44%	13.08%	5.75%	2.73%	2.85%	2.55%
25	12.89%	27.02%	10.94%	5.38%	5.63%	5.04%
50	42.28%	53.94%	39.28%	10.69%	11.18%	10.01%
100	69.94%	71.01%	68.39%	21.32%	22.29%	19.94%
200	97.59%	85.68%	97.92%	75.16%	48.02%	72.22%

The antifungal data against *Fusarium oxysporum* reveals a clear dose-dependent increase in activity for the ligand and its copper(II) complexes, particularly Cu(L)Cl and Cu(L)Br. Fig. S10.

shows the Petri plate was used to assess the antifungal activity of the ligand and copper(II) complexes against *Fusarium oxysporum* and Table S12 shows the antifungal activity of the ligand and copper(II) complexes against *Fusarium oxysporum.* At the lowest tested concentration (0.5 mg/mL), the ligand shows moderate activity (34.11 ± 4.25%), while Cu(L)Cl and Cu(L)Br exhibit lower but comparable effects (24.52 ± 4.04% and 26.68 ± 2.97%, respectively). As the concentration increases to 1 mg/mL and 1.5 mg/mL, the antifungal efficacy improves significantly. The ligand reaches 53.16 ± 3.38% inhibition at 1.5 mg/mL, and both Cu(L)Cl (50.97 ± 3.19%) and Cu(L)Br (52.65 ± 3.37%) show near-equal effectiveness (Fig. 10.).

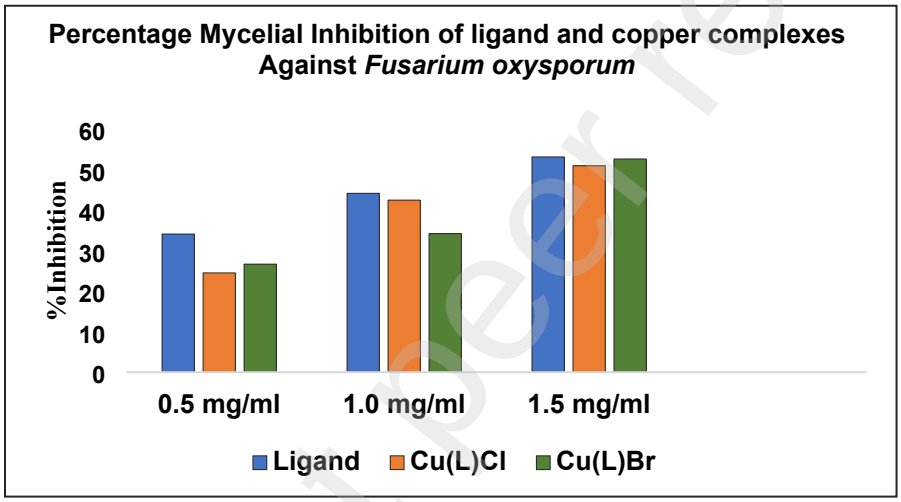

Fig. 10. Percentage Mycelial Inhibition of ligand and copper complexes Against *Fusarium oxysporum*

The DPPH approach is among the most straightforward and commonly used methods for measuring antioxidant activity. The hydrogen atom of the antioxidant molecule reduces the unpaired valence electron on the nitrogen atom in the DPPH radical. This leads to the developed of DPPH-H hydrazine[57]. By analyzing the absorbance decreased at 517 nm, spectrophotometric research can measure the amount of quenched DPPH radicals[58]. The IC_{50}, or the quantity of antioxidants needed to reduce the initial concentration of DPPH free radicals by 50%, is a measure of antioxidant activity[59–61]. The highest antioxidant activity is exhibited by the ligand (ABDHB because two hydroxyl groups are present, with an IC_{50} value of 1.12×10^{-4} g/ml in comparison of Cu(L)Cl (2.83×10^{-4} g/ml) and Cu(L)Br (3.08×10^{-4} g/ml) . The great binding stability and efficient electron-donating ability of the copper complexes with halides (Cu(L)Cl and Cu(L)Br) indicate a higher potential for antioxidant activity[62]. The ligand and copper (II) complexes are depicted

graphically in Fig. S11. The graphs show the concentration (x-axis) and the percentage of inhibition (y-axis).

The free ligand with two hydroxyl groups demonstrated the highest antifungal, anti-inflammatory, and antioxidant activity, owing to its increased ability to donate hydrogen atoms, chelate metal ions, and stabilize free radicals. Furthermore, the presence of two -OH groups increases the probability of hydrogen bonding with biological targets, hence intensifying the pharmacological response [55,63,64]. The Cu(L)Cl complex, which kept one hydroxyl group, was moderately active, whereas the Cu(L)Br complex, which had higher lipo changed electronic effects due to bromide coordination and restricted hydroxyl accessibility, was relatively good active.

4.4. Molecular Docking

Homeostasis and proper breast growth depend on apoptosis. In healthy breast epithelial cells, pro- and anti-apoptotic signals are strictly controlled. Breast cancer develops when this balance is disrupted, which raises the developed resistance to medicines including radiation, chemotherapy, and molecularly targeted therapies. 2W3L is a member of the pro- or anti-apoptotic BCL-2 protein family, which includes other important regulators of the apoptotic process. As a result, 2W3L is a promising target for increasing the killing of breast cancer tumor cells [65–67]. The docking procedure involved simulating the interaction of biologically active chemicals with two types of breast cancer proteins (PDB = 2W3L). A cellular stress protein called heme oxygenase-1 (HO-1) plays a role in the oxidative breakdown of heme, which produces carbon monoxide (CO), free iron, and biliverdin (BV). In this process, the generated BV is quickly converted to the powerful antioxidant bilirubin (BR), which is then turned back into BV by interacting with and neutralizing ROS. Consequently, HO-1 is a focus of research because of its ability to control oxidative and inflammatory processes, which enhances its effectiveness in treating metabolic diseases [58].

Table S13 displays the molecular docking results with bounded amino acid of protein with ligand and copper complex. Fig. 12. and Fig. 13. illustrate the 2D visualization of the interaction between the ligand (ABDHB), Cu(L)Cl, and Cu(L)Br with bcl-2 and HO-1. Cu(L)Cl has a good docking score of –6.06 kcal/mol against Bcl2-xL (2W3L), and the ligand (ABDHB) has a docking score of -7.89 kcal/mol against HO-1 (PDBI; 1N3U). These values demonstrate that the Cu(L)Cl and Ligand (ABDHB) are nicely fitted in the active pocket of the targeted

protein. In this case, the docking analysis supports the good anticancer and antioxidant activity results.

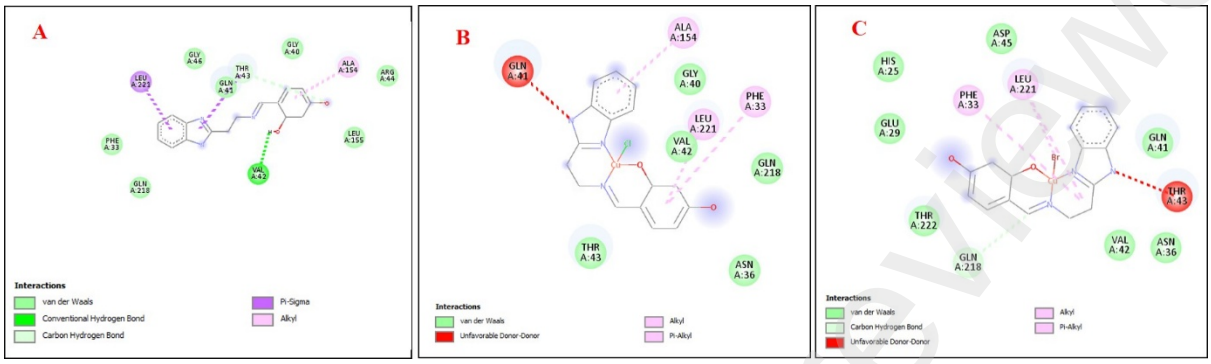

Fig. 12. The 2D visualization of molecular interaction of Bcl2-xL with Ligand (AB-DHB) (A), Cu(L)Cl (B), and Cu(L)Br (C) on protein (PDBI ID; 2W3L).

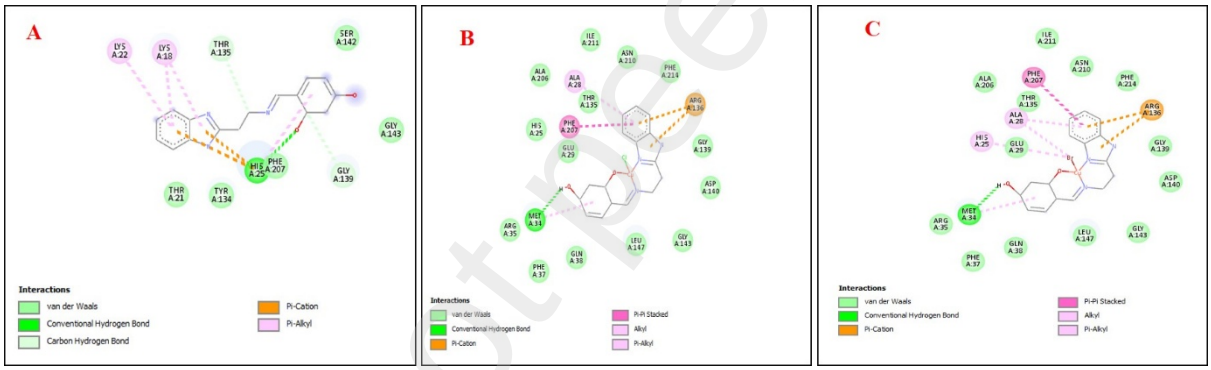

Fig. 13. The 2D visualization of molecular interaction of heme oxygenase-1 with Ligand (AB-DHB) (A), Cu(L)Cl (B), and Cu(L)Br (C) on protein (PDBI ID; 1N3U).

5. Conclusions

The presented work reports a new benzimidazole-based ligand and its copper(II) complexes with Cl^-, and Br^-, as counter ions. The tridentate nature of ligand with counter ions shows a distorted square bipyramidal nature of the metal complex. The ligand and its copper complexes, demonstrate a broad variety of bioactivities—anticancer, anti-inflammatory, antifungal, and antioxidant—that are closely correlated through their structural features and coordination chemistry. In anticancer assays against MCF-7 cells, Cu(L)Cl demonstrates the highest cytotoxicity, significantly outperforming the free ligand, and Cu(L)Br, likely due to lipophilic character of the central metal atom, enhanced cellular uptake, redox cycling, and ROS

generation. In anti-inflammatory studies, all compounds show dose-dependent inhibition of cytokines (TNF-α and IL-6), with Cu(L)Cl being most potent at intermediate concentrations, while at higher doses (200 μg/mL), both the ligand (99.30%) and Cu(L)Br (99.51%) nearly completely suppress TNF-α, indicating that metal-ligand synergy and halide lipophilicity contribute to cytokine modulation. Antifungal activity against *Fusarium oxysporum* similarly improves with concentration, where the ligand (53.16%), Cu(L)Br (52.65%), and Cu(L)Cl (50.97%) show comparable inhibition at 1.5 mg/mL, suggesting that copper coordination maintains or slightly enhances antifungal efficacy. In antioxidant assays using DPPH, the ligand shows the highest activity ($IC_{50} = 1.12\times10^{-4}$ g/mL). The free ligand with two hydroxyl groups exhibited the strongest anti-inflammatory, antifungal, and antioxidant activity, which can be attributed to its improved capacity to donate hydrogen atoms, chelate metal ions, and stabilize free radicals. Additionally, the presence of two -OH groups enhances the possibility of hydrogen bonding with biological targets, which intensifies the pharmacological response. Overall, the copper complexes, especially Cu(L)Cl, show superior anticancer and moderate-to-strong antifungal and anti-inflammatory activities, while the free ligand remains the strongest antioxidant, highlighting the influence of structural and electronic modifications across biological functions. The morphological observations from SEM provide substantial support for these conclusions. Along with its superior activity, the ligand's rod-like, clustered, porous shape and rough surface roughness probably help to improve biomolecular contacts and surface reactivity. The modest effectiveness of Cu(L)Cl, on the other hand, can be explained by the partial loss of reactive sites shown by its aggregated cube-like crystalline structures with decreased porosity. The decreased activity of the Cu(L)Br complex, on the other hand, can be explained by the fact that it showed compact rectangular plate-like crystals with smoother surfaces and lower surface roughness, which limits functional group exposure and reduces biological interactions. The observed activity pattern can be directly linked to these structural and morphological changes, and these findings collectively show that the number of hydroxyl groups and the surface morphology, as shown by SEM, work in concert to control the biological efficacy of these compounds. Molecular docking studies also supported the experimental data, where Cu(L)Cl showed strong binding to the anti-apoptotic Bcl-2 protein (2W3L) and the ligand exhibited high affinity toward HO-1 (1N3U). Collectively, these findings suggest that metal complexation with the ligand not only diversifies but also amplifies its biological potential, especially for anticancer and anti-inflammatory applications, while retaining

useful antioxidant and antifungal properties—making these compounds promising candidates for further pharmacological development.

Acknowledgements

The authors are thankful to UGC-BSR project no. 30-496/2019 and UCOST, Govt. of Uttarakhand, (project no. UCOST-RND/12/2024-UCOST-DPT-26322) for financial support. One of the authors (PK) sincerely thanks the UGC for the senior research fellowship. We gratefully acknowledge Gurukula Kangri (Deemed to be University), Haridwar for providing lab facilities and other resources. The authors are grateful to Dr. Kisan, Department of Chemistry, Gurukula Kangri (Deemed to be University), Haridwar, for his great working together with executing the molecular docking study.

Author contributions

Conceptualization and design: PK, VK, RK; Data curation and formal analysis: PK, KM, M, P, R, AKM, SKB, PKN, RK; Investigation and Methodology: PK, VK, AKM, RK; Manuscript writing and editing: All authors; Project administration and supervision: PK, AKM, RK.

Conflict of Interest

No conflicts of interest are disclosed by the authors.

Data Availability Statement

The study's supporting data may be found in the article's supplementary material. Crystal information for $C_{16}H_{15}N_3O_2$ in CIF format. The supplemental crystallographic data for this paper are contained in CCDC-2482799. The Cambridge Crystallographic Data Centre provides free access to this data at www.ccdc.cam.ac.uk/data_request/cif.

Ethical approval

Not Applicable

References

[1] H.S. Salem, Cancer status in the Occupied Palestinian Territories: types; incidence; mortality; sex, age, and geography distribution; and possible causes, J Cancer Res Clin Oncol 149 (2023) 5139–5163. https://doi.org/10.1007/s00432-022-04430-2.

[2] T. Tang, N. Liu, L. Wang, K. Zuo, X. Zhu, A Dual Bispecific Hydrolysis Peptide-Drug Conjugate Responsive to Micro-Acidic and Reduction Circumstance Promotes Antitumor Efficacy in Triple-Negative Breast Cancer, ChemBioChem 25 (2024). https://doi.org/10.1002/cbic.202400426.

[3] X. Bi, X. Chen, H. Li, Z. Fang, J. Cao, J. Hai, Nonmetal Methoxy-Porphyrin Nanophotosensitizers: An Antitumor Agent for Photodynamic Therapy against Breast Cancer and Cervical Cancer, ChemBioChem (2025). https://doi.org/10.1002/cbic.202500154.

[4] A.B. Nassif, M.A. Talib, Q. Nasir, Y. Afadar, O. Elgendy, Breast cancer detection using artificial intelligence techniques: A systematic literature review, Artif Intell Med 127 (2022) 102276. https://doi.org/10.1016/j.artmed.2022.102276.

[5] L. Tabár, P.B. Dean, F. Lee Tucker, O. Puchkova, R. Bozó, A. Ming-Fang Yen, S. Li-Sheng Chen, R.A. Smith, S.W. Duffy, T. Hsiu-Hsi Chen, The challenging imaging and histopathologic features of diffusely infiltrating breast cancer, Eur J Radiol 161 (2023) 110754. https://doi.org/10.1016/j.ejrad.2023.110754.

[6] P. Kaushik, B.S. Rawat, R. Kumar, Various approaches for the synthesis of benzimidazole derivatives and their catalytic application for organic transformation, Applied Chemical Engineering 6 (2023) 2003. https://doi.org/10.24294/ace.v6i2.2003.

[7] M. Mavvaji, S. Akkoc, Recent Advances in the Anticancer Applications of Benzimidazole Derivatives, ChemistrySelect 8 (2023). https://doi.org/10.1002/slct.202302561.

[8] A. Choudhary, R.H. Viradiya, R.N. Ghoghari, K.H. Chikhalia, Recent Scenario for the Synthesis of Benzimidazole Moiety(2020–2022), ChemistrySelect 8 (2023). https://doi.org/10.1002/slct.202204910.

[9] M. Türkmenoğlu, S.T. Yıldırım, A. Altay, B. Türkmenoğlu, Synthesis, Characterization, Investigation of Anticancer Activity and Molecular Docking Studies of N_2O_2 Type Schiff Base Ligand and Metal Complexes, ChemistrySelect 9 (2024). https://doi.org/10.1002/slct.202303519.

[10] G. Ahuja, R. Kumar, P. Mathur, Oxidation of olefins catalyzed by Iron (III) complexes of bis-benzimidazolyl diamide ligands, J Mol Struct 1011 (2012) 166–171. https://doi.org/10.1016/j.molstruc.2011.12.047.

[11] N. Tyagi, R. Kumar, K. Mahiya, P. Mathur, Copper(II) complexes of a new tetradentate *bis* -benzimidazolyl diamide ligand with disulfanediyl linker: synthesis, characterization, and oxidation of some pyridyl, napthyl, and benzyl alcohols, J Coord Chem 66 (2013) 3335–3348. https://doi.org/10.1080/00958972.2013.835403.

[12] R. Kumar, K. Mahiya, P. Mathur, Dimeric copper(ii) complex of a new Schiff base ligand: Effect of morphology on the catalytic oxidation of aromatic alcohol, Dalton Transactions 42 (2013) 8553. https://doi.org/10.1039/c3dt50348h.

[13] K. Mahiya, R. Kumar, F. Lloret, P. Mathur, Oxidation of substituted phenols using copper(II) metallatriangles formed through ligand sharing, Spectrochim Acta A Mol Biomol Spectrosc 133 (2014) 663–668. https://doi.org/10.1016/j.saa.2014.06.026.

[14] R. Kumar, P. Mathur, Aerobic oxidation of 1,10-phenanthroline to phen-dione catalyzed by copper(<scp>ii</scp>) complexes of a benzimidazolyl Schiff base, RSC Adv 4 (2014) 33190. https://doi.org/10.1039/C4RA03651D.

[15] R. Kumar, R. Kumar, K. Mahiya, P. Mathur, Oxidation of substituted benzyl amines using a phenoxo-bridged dimeric nickel(II) complex: synthesis, crystal structure and catalytic activity, Transition Metal Chemistry 40 (2015) 189–195. https://doi.org/10.1007/s11243-014-9905-y.

[16] R. Kumar, P. Mathur, Oxidation of phenyl propyne catalyzed by copper(II) complexes of a benzimidazolyl schiff base ligand: Effect of acid/base, oxidant, surfactant and morphology, Spectrochim Acta A Mol Biomol Spectrosc 136 (2015) 818–823. https://doi.org/10.1016/j.saa.2014.09.099.

[17] R. Kumar, A. Yadav, K. Mahiya, P. Mathur, Copper(II) complexes with box or flower type morphology: Sustainability versus perishability upon catalytic recycling, Inorganica Chim Acta 450 (2016) 279–284. https://doi.org/10.1016/j.ica.2016.06.012.

[18] P. Kaushik, N. Malik, P. Tevatia, V. Kumar, P.K. Sahu, R. Kumar, Morphology based catalytic oxidation of phenylpropyne into 1,2-diketones, aldehyde and acid using Cu(II) complex, Applied Chemical Engineering 6 (2023). https://doi.org/10.24294/ace.v6i3.2009.

[19] N.C. Desai, K.N. Shah, J. Monapara, B.P. Dave, I. Ahmad, H. Patel, "Design, synthesis, biological profile and molecular modeling and MD simulation studies of heterocyclic benzimidazole and thiazolidine-4-one based 5-arylidene analogues as prospective

antimicrobial agents," J Mol Struct 1299 (2024) 137166. https://doi.org/10.1016/j.molstruc.2023.137166.

[20] M. Kumar, A.K. Singh, S. Singh, A.K. Singh, P.K. Rao, R.K. Yadav, A.P. Singh, U.N. Tripathi, Exploration of iron(III) complexes with bidentate N, O-donor Schiff base ligands through synthesis, characterization, DFT, and antibacterial studies, J Mol Struct 1319 (2025) 139496. https://doi.org/10.1016/j.molstruc.2024.139496.

[21] A.M. Mansour, K. Radacki, O.R. Shehab, G.A.E. Mostafa, E.A. Ali, M.T. Abo-Elfadl, Pd(II) complexes of 2,6-bis(1-ethyl-benzimidazol-2′-yl)pyridine and 4-((pyridin-2-ylmethylene)amino)aniline: antiproliferative properties and mechanism of action, J Mol Struct 1348 (2025) 143457. https://doi.org/10.1016/j.molstruc.2025.143457.

[22] O. Omotuyi, O.M. Olatunji, O. Nash, B. Oyinloye, O. Soremekun, A. Ijagbuji, S. Fatumo, Benzimidazole compound abrogates SARS-COV-2 receptor-binding domain (RBD)/ACE2 interaction In vitro, Microb Pathog 176 (2023) 105994. https://doi.org/10.1016/j.micpath.2023.105994.

[23] E. Arslan, Z.P. Haslak, G. Monard, I. Dogan, V. Aviyente, Quantum Mechanical Prediction of Dissociation Constants for Thiazol-2-imine Derivatives, J Chem Inf Model 63 (2023) 2992–3004. https://doi.org/10.1021/acs.jcim.2c01468.

[24] R. Radhamanalan, M. Alagumuthu, N. Nagaraju, Synthesis and drug efficacy validations of racemic-substituted benzimidazoles as antiulcer/antigastric secretion agents, Future Med Chem 10 (2018) 1805–1820. https://doi.org/10.4155/fmc-2017-0214.

[25] A.-M. Monforte, S. Ferro, L. De Luca, G. Lo Surdo, F. Morreale, C. Pannecouque, J. Balzarini, A. Chimirri, Design and synthesis of N1-aryl-benzimidazoles 2-substituted as novel HIV-1 non-nucleoside reverse transcriptase inhibitors, Bioorg Med Chem 22 (2014) 1459–1467. https://doi.org/10.1016/j.bmc.2013.12.045.

[26] N. Anastassova, D. Aluani, N. Hristova-Avakumova, V. Tzankova, M. Kondeva-Burdina, M. Rangelov, N. Todorova, D. Yancheva, Study on the Neuroprotective, Radical-Scavenging and MAO-B Inhibiting Properties of New Benzimidazole Arylhydrazones as Potential Multi-Target Drugs for the Treatment of Parkinson's Disease, Antioxidants 11 (2022) 884. https://doi.org/10.3390/antiox11050884.

[27] S. V. Bhandari, O.G. Nagras, P. V. Kuthe, A.P. Sarkate, K.S. Waghamare, D.N. Pansare, S.Y. Chaudhari, S.N. Mawale, M.C. Belwate, Design, Synthesis, Molecular Docking and

Antioxidant Evaluation of Benzimidazole-1,3,4 oxadiazole Derivatives, J Mol Struct 1276 (2023) 134747. https://doi.org/10.1016/j.molstruc.2022.134747.

[28] W. V. Ferreira, F.R. Ráice, A.F. da Silva, I.J. Nunes, R. Cervo, R. Cargnelutti, J. Saffi, J.L.S. Milani, O. de L. Casagrande, A.C. Pinheiro, Synthesis, characterization, electronic properties, and cytotoxic activities on cancer cells line of novel Cu(II) complexes with benzimidazole-Schiff base tridentate ligand, J Mol Struct 1327 (2025) 141239. https://doi.org/10.1016/j.molstruc.2024.141239.

[29] A. Shakoor, G. Fareed, I. Ahmad, A.A. Elhenawy, M. Khan, N. Fareed, E. Al-Olayan, M.R. Abukhadra, A. Alam, M. Ibrahim, Exploring the anti-diabetic activity of benzimidazole containing Schiff base derivatives: In vitro α-amylase, α-glucosidase inhibitions and in silico studies, J Mol Struct 1321 (2025) 140136. https://doi.org/10.1016/j.molstruc.2024.140136.

[30] M. Khalifa, A. Gobouri, F. Kabli, T. Altalhi, A. Almalki, M. Mohamed, Synthesis, Antibacterial, and Anti HepG2 Cell Line Human Hepatocyte Carcinoma Activity of Some New Potentially Benzimidazole-5-(Aryldiazenyl)Thiazole Derivatives, Molecules 23 (2018) 3285. https://doi.org/10.3390/molecules23123285.

[31] J.E. Cheong, M. Zaffagni, I. Chung, Y. Xu, Y. Wang, F.E. Jernigan, B.R. Zetter, L. Sun, Synthesis and anticancer activity of novel water soluble benzimidazole carbamates, Eur J Med Chem 144 (2018) 372–385. https://doi.org/10.1016/j.ejmech.2017.11.037.

[32] G. Bairy, C. Sinha, An Extensive Analysis of Current Synthetic Methodologies and Applications of Imidazo/Benzimidazo[1,2- *c*]Quinazolines, ChemistrySelect 9 (2024). https://doi.org/10.1002/slct.202400421.

[33] J.P. Rada, J. Forté, G. Gontard, V. Corcé, M. Salmain, N.A. Rey, Isoxazole-Derived Aroylhydrazones and Their Dinuclear Copper(II) Complexes Show Antiproliferative Activity on Breast Cancer Cells with a Potentially Alternative Mechanism Of Action, ChemBioChem 21 (2020) 2474–2486. https://doi.org/10.1002/cbic.202000122.

[34] A.P.A. Oliveira, A.A. Recio-Despaigne, I.P. Ferreira, R. Diniz, K.A.F. Sousa, T.M. Bastos, M.B. Pereira Soares, D.R.M. Moreira, H. Beraldo, Investigation of the antitrypanosomal effects of 2-formyl-8-hydroxyquinoline-derived hydrazones and their antimony(<scp>iii</scp>) and bismuth(<scp>iii</scp>) complexes, New Journal of Chemistry 43 (2019) 18996–19002. https://doi.org/10.1039/C9NJ02676B.

[35] C.-H. Li, J.-H. Jiang, Y.-H. Lei, X. Li, F.-H. Yao, M.-H. Ji, K.-W. Zhang, L.-M. Tao, L.-J. Ye, Q.-G. Li, Design, synthesis, and biological evaluation of dinuclear bismuth(III) complexes with Isoniazid-derived Schiff bases, J Inorg Biochem 235 (2022) 111931. https://doi.org/10.1016/j.jinorgbio.2022.111931.

[36] C. Immanuel David, P.T. Movuleeshwaran, H. Jayaraj, G. Prabakaran, D. Parimala devi, M.S. Kumar, A. Abiram, T.G. Satheesh Babu, J. Prabhu, R. Nandhakumar, Highly selective, reversible and ICT-based fluorescent chemosensor for bismuth ions: Applications in bacterial imaging, logic gate and food sample analysis, J Photochem Photobiol A Chem 422 (2022) 113558. https://doi.org/10.1016/j.jphotochem.2021.113558.

[37] M.S. Sinicropi, J. Ceramella, D. Iacopetta, A. Catalano, A. Mariconda, C. Rosano, C. Saturnino, H. El-Kashef, P. Longo, Metal Complexes with Schiff Bases: Data Collection and Recent Studies on Biological Activities, Int J Mol Sci 23 (2022) 14840. https://doi.org/10.3390/ijms232314840.

[38] S. Khan, F.A. Alhumaydhi, M.M. Ibrahim, A. Alqahtani, M. Alshamrani, A.S. Alruwaili, A.A. Hassanian, S. Khan, Recent Advances and Therapeutic Journey of Schiff Base Complexes with Selected Metals (Pt, Pd, Ag, Au) as Potent Anticancer Agents: A Review, Anticancer Agents Med Chem 22 (2022) 3086–3096. https://doi.org/10.2174/1871520622666220511125600.

[39] I. Santos Oliveira, C. Marrote Manzano, D. Hideki Nakahata, M. Brentini Santiago, N. Bernadelli Sousa Silva, C. Henrique Gomes Martins, F. Pimentel Respíndula, D. Henrique Pereira, P. Paulo Corbi, Antibacterial and antifungal activities in vitro of a novel silver(I) complex with sulfadoxine-salicylaldehyde Schiff base, Polyhedron 225 (2022) 116073. https://doi.org/10.1016/j.poly.2022.116073.

[40] A. Oveisi Keikha, S. Shahraki, H. Mansouri-Torshizi, E. Dehghanian, M. Heidari Majd, Au(III) complexes of symmetrical tetradentate Schiff base ligands: Synthesis, characterization, anticancer/antioxidant potency, in silico prediction, and catalase binding properties, Appl Organomet Chem 37 (2023). https://doi.org/10.1002/aoc.7139.

[41] J. Szklarzewicz, A. Jurowska, M. Hodorowicz, G. Kazek, B. Mordyl, E. Menaszek, J. Sapa, Characterization and antidiabetic activity of salicylhydrazone Schiff base vanadium(IV) and (V) complexes, Transition Metal Chemistry 46 (2021) 201–217. https://doi.org/10.1007/s11243-020-00437-1.

[42] M. Gaber, N. El-Wakiel, O.M. Hemeda, Cr(III), Mn(II), Co(II), Ni(II) and Cu(II) complexes of 7-((1H-benzo[d]imidazol-2-yl)diazenyl)-5-nitroquinolin-8-ol.synthesis, thermal, spectral, electrical measurements, molecular modeling and biological activity, J Mol Struct 1180 (2019) 318–329. https://doi.org/10.1016/j.molstruc.2018.12.006.

[43] M. Moreno-Alvero, F. Luna-Giles, F.J. Barros-García, E. Viñuelas-Zahínos, M.C. Fernández-Calderón, Cobalt(II) complexes derived from a 2-aminobenzimidazole-thiazoline ligand: Synthesis, characterization, crystal structures and antimicrobial activity studies, Polyhedron 207 (2021) 115390. https://doi.org/10.1016/j.poly.2021.115390.

[44] L.A. CESCON, A.R. DAY, Preparation of Some Benzimidazolylamino Acids. Reactions of Amino Acids with o-Phenylenediamines, J Org Chem 27 (1962) 581–586. https://doi.org/10.1021/jo01049a056.

[45] A.M.A. El-Seidy, E. El-Zahany, A.S. Barakat, N.S. Youssef, S.A. Galal, S.A. Drweesh, Synthesis, Characterization, and Cytotoxic Activity on MCF-7 Cell Line of Some Novel Metal Complexes With Substituted Benzimidazole Ligands, Synthesis and Reactivity in Inorganic, Metal-Organic, and Nano-Metal Chemistry 43 (2013) 46–56. https://doi.org/10.1080/15533174.2012.682691.

[46] O.M.I. Adly, H.F. El-Shafiy, New metal complexes derived from *S* -benzyldithiocarbazate (SBDTC) and chromone-3-carboxaldehyde: synthesis, characterization, antimicrobial, antitumor activity and DFT calculations, J Coord Chem 72 (2019) 218–238. https://doi.org/10.1080/00958972.2018.1564912.

[47] A. Gómez-Lopez, Y.A. Rivas, S. López-Fajardo, R. Jiménez, J. Ricote, C. Pecharromán, I. Montero, I. Bretos, M.L. Calzada, *In situ* photogenerated hydroxyl radicals in the reaction atmosphere for the accelerated crystallization of solution-processed functional metal oxide thin films, J Mater Chem C Mater 11 (2023) 2619–2629. https://doi.org/10.1039/D2TC05447G.

[48] D. Sek, M. Siwy, K. Bijak, M. Grucela-Zajac, G. Malecki, K. Smolarek, L. Bujak, S. Mackowski, E. Schab-Balcerzak, Comparative Studies of Structural, Thermal, Optical, and Electrochemical Properties of Azines with Different End Groups with Their Azomethine Analogues toward Application in (Opto)Electronics, J Phys Chem A 117 (2013) 10320–10332. https://doi.org/10.1021/jp407623u.

[49] Y.M. Issa, H.B. Hassib, H.E. Abdelaal, 1H NMR, 13C NMR and mass spectral studies of some Schiff bases derived from 3-amino-1,2,4-triazole, Spectrochim Acta A Mol Biomol Spectrosc 74 (2009) 902–910. https://doi.org/10.1016/j.saa.2009.08.042.

[50] B. Delley, An all-electron numerical method for solving the local density functional for polyatomic molecules, J Chem Phys 92 (1990) 508–517. https://doi.org/10.1063/1.458452.

[51] S. Grimme, J. Antony, S. Ehrlich, H. Krieg, A consistent and accurate *ab initio* parametrization of density functional dispersion correction (DFT-D) for the 94 elements H-Pu, J Chem Phys 132 (2010). https://doi.org/10.1063/1.3382344.

[52] J.P. Perdew, K. Burke, M. Ernzerhof, Generalized Gradient Approximation Made Simple, Phys Rev Lett 77 (1996) 3865–3868. https://doi.org/10.1103/PhysRevLett.77.3865.

[53] Mandeep, A. Gulati, Jogender, R. Kakkar, DFT study of carbaryl pesticide adsorption on vacancy and nitrogen-doped graphene decorated with platinum clusters, Struct Chem 32 (2021) 1541–1551. https://doi.org/10.1007/s11224-020-01693-8.

[54] Anju, S. Chaturvedi, V. Chaudhary, P. Pant, P. Jha, S.S. Kumaran, F. Hussain, A. Kumar Mishra, 5-HT1A targeting PARCEST agent DO3AM-MPP with potential for receptor imaging: Synthesis, physico-chemical and MR studies, Bioorg Chem 106 (2021) 104487. https://doi.org/10.1016/j.bioorg.2020.104487.

[55] M.S. Alam, J.-H. Choi, D.-U. Lee, Synthesis of novel Schiff base analogues of 4-amino-1,5-dimethyl-2-phenylpyrazol-3-one and their evaluation for antioxidant and anti-inflammatory activity, Bioorg Med Chem 20 (2012) 4103–4108. https://doi.org/10.1016/j.bmc.2012.04.058.

[56] R. Wilcken, M.O. Zimmermann, A. Lange, A.C. Joerger, F.M. Boeckler, Principles and Applications of Halogen Bonding in Medicinal Chemistry and Chemical Biology, J Med Chem 56 (2013) 1363–1388. https://doi.org/10.1021/jm3012068.

[57] Kishan, R.K. Shukla, A. Shukla, R. Singh, PROXIMATE ANALYSIS, PHYTOCHEMICAL SCREENING, TOTAL PHENOLIC CONTENT AND In-Vitro ANTIOXIDANT POTENTIAL OF Prunus domestica L. (SEED COAT), Rasayan Journal of Chemistry 15 (2022) 239–250. https://doi.org/10.31788/RJC.2022.1516495.

[58] K. Chkirate, G. Al Ati, K. Karrouchi, S. Fettach, H. Chakchak, J.T. Mague, S. Radi, N.N. Adarsh, M. El Abbes Faouzi, E.M. Essassi, Y. Garcia, Cu ^{II} Pyrazolyl-Benzimidazole

Dinuclear Complexes with Remarkable Antioxidant Activity, ChemBioChem 24 (2023). https://doi.org/10.1002/cbic.202300331.

[59] R.K. Shukla, Kishan, A. Shukla, R. Singh, Evaluation of nutritive value, phytochemical screening, total phenolic content and in-vitro antioxidant activity of the seed of Prunus domestica L., Plant Science Today 8 (2021). https://doi.org/10.14719/pst.2021.8.4.1231.

[60] R.K. Shukla, Kishan, A. Shukla, Zinc Oxide Nanorods from Prunus domestica L.: Bio-Assisted Synthesis, Characterization, Antioxidant and Cytotoxic Activities, Indian J Biochem Biophys (2025). https://doi.org/10.56042/ijbb.v62i1.12810.

[61] Kishan, R.K. Shukla, A. Shukla, A. Budhlakoti, Therapeutic Potentials of Characterized Isolate from Column Chromatography by GC-MS and Molecular Docking of Principle Active of Prunus domestica L., Indian J Chem 63 (2024). https://doi.org/10.56042/ijc.v63i7.7567.

[62] L. Esmaeili, M.G. Perez, M. Jafari, J. Paquin, P. Ispas-Szabo, V. Pop, M. Andruh, J. Byers, M.A. Mateescu, Copper complexes for biomedical applications: Structural insights, antioxidant activity and neuron compatibility, J Inorg Biochem 192 (2019) 87–97. https://doi.org/10.1016/j.jinorgbio.2018.12.010.

[63] B. Bano, K.M. Khan, A. Jabeen, A. Hameed, A. Faheem, M. Taha, S. Perveen, S. Iqbal, Aminoquinoline Schiff Bases as Non-Acidic, Non-Steroidal, Anti-Inflammatory Agents, ChemistrySelect 2 (2017) 10050–10054. https://doi.org/10.1002/slct.201702200.

[64] P. Borrego-Muñoz, F. Ospina, D. Quiroga, A Compendium of the Most Promising Synthesized Organic Compounds against Several Fusarium oxysporum Species: Synthesis, Antifungal Activity, and Perspectives, Molecules 26 (2021) 3997. https://doi.org/10.3390/molecules26133997.

[65] S. Gomha, S. Riyadh, B. Huwaimel, M. Zayed, M. Abdellattif, Synthesis, Molecular Docking Study, and Cytotoxic Activity against MCF Cells of New Thiazole–Thiophene Scaffolds, Molecules 27 (2022) 4639. https://doi.org/10.3390/molecules27144639.

[66] M.M. Williams, R.S. Cook, Bcl-2 family proteins in breast development and cancer: could Mcl-1 targeting overcome therapeutic resistance?, Oncotarget 6 (2015) 3519–3530. https://doi.org/10.18632/oncotarget.2792.

[67] N. Sathishkumar, S. Sathiyamoorthy, M. Ramya, D.-U. Yang, H.N. Lee, D.-C. Yang, Molecular docking studies of anti-apoptotic BCL-2, BCL-XL, and MCL-1 proteins with

ginsenosides from *Panax ginseng*, J Enzyme Inhib Med Chem 27 (2012) 685–692. https://doi.org/10.3109/14756366.2011.608663.